DOI 10.1007/s10812-021-01219-y
*Journal of Applied Spectroscopy, Vol. 88, No. 3, July, 2021 (Russian Original Vol. 88, No. 3, May–June, 2021)*

# THE CRYSTAL STRUCTURE, SPECTRAL, AND DENSITY FUNCTIONAL THEORY STUDIES OF [3-(3-BROMOPHENYL)-*cis*-4,5-DIHYDROISOXAZOLE-4,5-DIYL]bis(METHYLENE)DIACETATE

**Y. S. Kara,* A. Eşme, and S. G. Sagdinc**

UDC 548.0;539.143.43

*The crystal structure of [3-(3-bromophenyl)-cis-4,5-dihydroisoxazole-4,5-diyl]bis(methylene)diacetate (BDBD) was determined using X-ray diffraction data. Hirschfeld surface and fingerprint plots were used to locate and analyze the molecular surface. The optimized molecular structures, frontier molecular orbitals, quantum chemical parameters, and NMR chemical shifts of the investigated compound were calculated with DFT at the B3LYP/6-311G(d,p) level of theory. The experimental NMR of the studied compound was measured in deuterochloroform ($CDCl_3$) solvent, employing tetramethylsilane as an internal standard. It was established that the experimental and simulated $^1H$ and $^{13}C$ NMR spectra were in good agreement. Vibrational spectrum analysis was carried out by FT-IR spectroscopy in the range 400–4000 $cm^{-1}$ for the title molecule. The vibrational frequencies of the investigated compound were calculated with DFT at the B3LYP/6-311G(d,p) level of the theory. The wavenumbers received complete vibrational assignments based on their potential energy distribution. The experimental and simulated FT-IR spectra were in good agreement.*

***Keywords:*** *X-ray crystal structure, Hirschfeld surface analysis, density functional theory, isoxazole, nuclear magnetic resonance, Fourier-transform infrared spectroscopy.*

**Introduction.** Isoxazole and its derivatives have a long history of application in pharmaceuticals and natural bioactive products. In particular, 4,5-dihydroisoxazoles show antimicrobial, antifungal, estrogen receptor β, antiarthritic, anti-inflammatory, analgesic, antibacterial, and anthelmintic effects [1–5]. The most useful method to prepare a 4,5-dihydroisoxazole compound involves the 1,3-dipolar cycloaddition reaction with nitrile oxides and olefins. In our previous study, we synthesized 11 novel [3-(substituted phenyl)-*cis*-4,5-dihydroisoxazole-4,5-diyl]bis(methylene) diacetates and characterized them by FT-IR, $^1H$ NMR (nuclear magnetic resonance), $^{13}C$ NMR methods as well as by elemental analysis [6]. However, we did not conduct any detailed theoretical or spectroscopic analysis of any derivatives of [3-(substituted phenyl)-*cis*-4,5-dihydroisoxazole-4,5-diyl]bis(methylene)diacetate. Therefore, in this study, we describe the molecular structure of [3-(3-bromophenyl)-*cis*-4,5-dihydroisoxazole-4,5-diyl]bis(methylene)diacetate (BDBD), which is the *m*-bromo substituted derivative synthesized in our previous study [6]. We present the analysis of its X-ray crystal structure, optimized molecular structure, Hirschfeld surface, frontier molecular orbital, quantum chemical parameters, NMR spectra, and vibrational frequency.

**Experiment and Calculations.** *Materials and physical measurements.* Recently, we synthesized a BDBD compound [6]. The $^1H$ NMR and $^{13}C$ NMR chemical shifts of the investigated compound were recorded in deuterochloroform ($CDCl_3$) solutions, employing tetramethylsilane (TMS) as an internal standard. These spectra were recorded on a Bruker DPX-400 (400 MHz) high-performance digital FT-NMR spectrometer. The FT-IR spectrum of the studied molecule was recorded on a Bruker Alpha II ATR (attenuated total reflection) spectrometer in the range 400–4000 $cm^{-1}$.

*X-ray crystallographic study.* The single-crystal X-ray intensity data for BDBD, [$C_{15}H_{16}BrNO_5$], were measured on a Bruker D8 VENTURE diffractometer equipped with a PROTON 100 detector. Data were collected with a multilayer monochromator and a Mo$K_\alpha$ sealed tube (λ = 0.71073 Å) at 100(0) K using a Bruker Kryoflex II cooling attachment. Data were corrected for adsorption effects using the multi-scan method (SADABS) [7]. The structure was solved through the direct method using the SHELXS-1997 program [8] of SHELXTL software [9]. Molecular drawings were generated through PLATON [10] and ORTEP [11] and built using OLEX2. ver.1.2-dev [12].

Kocaeli University, 41380, Umuttepe, Kocaeli, Turkey; email: yesimkara69@gmail.com. Abstract of article is published in Zhurnal Prikladnoi Spektroskopii, Vol. 88, No. 3, p. 501, May–June, 2021.

*Calculation methods.* DFT was calculated using the Gaussian 09 Rev. A 11.4 package [13] and visualized using the Gauss View Rev. 5.0.9 software [14]. The X-ray parameter structure of BDBD (CCDC: 1976365) was used as the initial guess for geometry optimization. The molecular structure of the studied compound in the ground state (in the gaseous phase) was optimized with Becke's 3-parameter exchange–correlation functional using the Lee–Yang–Parr correlation functional (B3LYP) in the 6-311G(*d*,*p*) basis set [15, 16]. After the geometry optimization, the quantum chemical parameters were calculated with the same method. In the Gaussian 09 Rev. A 11.4 package program, the integral equation formalism for the polarizable continuum model (IEF-PCM) was used to perform the calculation in chloroform [17]. The detailed assignments of vibrational modes were based on the percentage potential energy distributions (PEDs) using the VEDA4 program [18].

**Results and Discussion.** *X-Ray and optimized molecular structure analysis.* A suitable clear-light-white needle-like single crystal of the BDBD compound, with dimensions 0.050 × 0.100 × 0.800 mm, was grown by slow evaporation of the ethanol solution at room temperature. X-ray diffraction analysis revealed that the title compound crystallized in a triclinic system. The data-collection conditions and the parameters of the refinement process are listed in Table 1.

The atomic numbering and optimized structure of the BDBD compound obtained by the density functional theory (DFT) at the B3LYP/6-311G(*d*,*p*) level are presented in Fig. 1. The studied compound consisted of three groups, an isoxazole ring, a phenyl ring, and acetate chains, which are not coplanar. Further details on the crystal data, collection, and refinements can be found in the supporting information in CCDC 1976365.

The geometric parameters for BDBD calculated by the DFT method at the B3LYP/6-311G(*d*,*p*) level are compared with the X-ray experimental parameters (Table 2). The bond lengths of the investigated molecular skeleton approximately coincide with the typical bond lengths (C–C, 1.54 Å; C–O, 1.43 Å; C=O, 1.21 Å; C=N, 1.25 Å; N–O, 1.40 Å) [19]. The C=O and C=N bonds are characteristic double bonds, so C=X (where X denotes O or N atoms) bonds are shorter than the single C–X bond length that results in resonance and electron delocalization between the bonds [14, 15]. The C12=O14 [1.206(2) Å] and C2=O5 bonds [1.192(2) Å] are typically C=O bonds, whereas C2=O5 has a slightly shorter bond length than C12=O14 due to steric and electronic effects (Table 2). The Br1–C9 bond distance [1.901(17) Å experimentally and 1.919 Å for B3LYP/6-311G(*d*,*p*) in the gaseous phase] is the longest in the studied molecule. However, the C2=O5 bond distance [1.192(2) Å experimentally and 1.202 Å for B3LYP/6-311G(*d*,*p*) in the gaseous phase] is the shortest, which indicates the localization of the electron density in this part of the molecule.

As seen in Table 2, the bond distance of C6=N1 was 1.285 (2) Å both experimentally and theoretically. In a previously report [20], the N–O bond length was 1.401 Å experimentally and 1.400 Å theoretically. As can be seen in Table 2, the bond length of N1–O2 is 1.418(18) Å experimentally and 1.390 Å theoretically in the gaseous phase. The N–O bond length in the studied compound was consistent with that found in the literature. The observed C–C bond lengths in the phenyl rings were in the range 1.380–1.401 Å, which is consistent with the previous studies involving phenyl rings [21].

The experimental and theoretical values of different bond angles showed very strong correlations with each other. The X-ray values of the bond angles for C10–C9–Br1, N1–C6–C7, O4–C12–O3, and O5–C2-C1 were 119.39 (13)$^{o}$, 121.01 (15)$^{o}$, 122.97 (16)$^{o}$, and 124.92 (16)$^{o}$, respectively. The theoretical values of these bond angles were observed at 119.08$^{o}$, 121.65$^{o}$, 123.42$^{o}$, and 125.77$^{o}$ in the gaseous phase, respectively.

The theoretical values of all dihedral angles showed good correlation with the experimental ones (Table 2). The experimental and calculated values of the dihedral angles for the phenyl ring are close to 0. Similarly, the experimental and theoretical values of the torsion angle for Br1–C9–C10–C14 for the gaseous phase are –178.92 (13)$^{o}$ and 179.99$^{o}$, respectively. This shows that the substituent Br is planar with the phenyl ring. The small difference between the calculated and experimental geometrical parameters can be explained by the conduction of the experiment in the solid state, whereas the theoretical values were obtained in the chloroform and gaseous phase.

*Hirschfeld surface analysis.* The nature of the intermolecular interactions and their quantitative contributions in the BDBD crystal were analyzed with the Hirschfeld surfaces ($d_{norm}$, shape index and curvedness) using Crystal Explorer 3.1 [22, 23].

The associated 2-dimensional (2D) fingerprint plots (FPs) of BDBD with its donor ($d_i$) and acceptor ($d_e$) regions were realized and plotted in Fig. 2a. The normalized contact distance $d_{norm}$ is a parameter that includes the $d_i$ and $d_e$ distances, representing the distance from the Hirschfeld surface to the nearest nucleus inside and outside the surface, respectively. The strong C=O···H interactions are visualized as light-red clouds between the respective donor and acceptor atoms on the Hirschfeld surface, which shows negative potentials around the O atoms.

The most important hydrogen bonds of BDBD are the H···H/H···H with a relative contribution of 38.0%. The relative contributions for O···H/H···O, C···H/H···C, Br···H/H···Br, and N···H/H···N bonds were 27.8, 10.8, 10.3 and 3.7%,

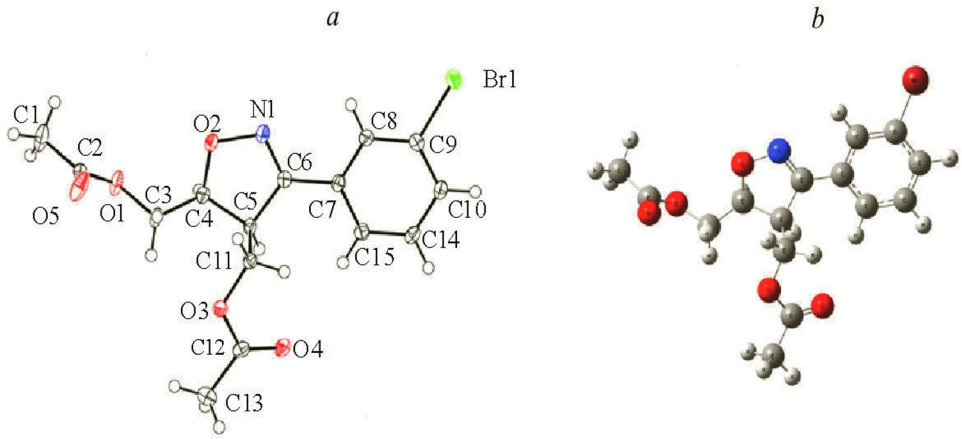


Fig. 1. a) The ORTEP diagram of BDBD compound. Displacements ellipsoids are shown at a 50% probability level; b) optimized structure obtained using B3LYP/6-311G(*d*,*p*) of BDBD

respectively. The H···H bonds appear as the largest region of the FP plot, with a high concentration in the middle region at $d_i = d_e \cong 1.3$ Å (Fig. 2e). The C···H/H···C interactions appear as the bottom-right ($d_i > d_e$) and top-left ($d_i < d_e$) regions of the FP plot and are highly concentrated at the edges, having almost the same values of $d_i + d_e \cong 3.1$ Å (Fig. 2f). Figure 2g shows that two pairs of symmetrical long spikes are present at $d_i + d_e \cong 2.4$ Å for the O···H/H···O interactions in the FPs.

*Frontier molecular orbitals and quantum chemical parameters.* The energies and distributions of the frontier molecular orbital (FMO) theory are very useful indicators of reactivity. HOMO and LUMO act as the donor and electron acceptor in the FMO theory, respectively, and are helpful for calculating the electric and optical parameters [24]. The 3D plots of HOMO and LUMO for BDBD obtained using the B3LYP/6-311G(*d*,*p*) method are shown in Fig. 3. As seen from Fig. 3, both HOMO and LUMO were mostly localized on the benzene and isoxazole rings. In addition, the HOMO orbital is localized in the Br atom.

The Gauss–Sum 2.2 program [25] was used to calculate the density of states (DOS) diagrams, which were drawn by plotting the molecular orbital data. Figure 3 shows the DOS diagram of the BDBD compound in the gaseous phase. The DOS plot gives the number of states per energy interval for both the virtual and occupied energy levels. The lines at the starting end of the energy axis of the plot, from –20 to –5 eV, are named occupied orbitals and those from –5 to 0 eV are named virtual orbitals.

The total energy of the BDBD compound was calculated as very close values in the gaseous and chloroform phases (–97593.249 versus –97593.546 eV). The $E_{HOMO}$ and $E_{LUMO}$ of the BDBD compound in the gaseous and chloroform phases are used to calculate the quantum chemical parameters, as shown in Table 3. The energies of HOMO are calculated as –6.563 and –6.614 eV in the gaseous and chloroform phases, respectively. The LUMO energies in the gaseous and chloroform phases are also calculated as –1.802 and –1.847 eV, respectively. The energy gap ($\Delta E_{HOMO–LUMO}$) between the HOMO and LUMO orbitals is a critical parameter in determining and understanding the molecular transport properties [26]. The energy gap for the BDBD compound was calculated as 4.761 and 4.767 eV in the gaseous and chloroform phases, respectively.

The ionization potential ($I$) and electron affinity ($A$) are related to the energies of the molecule HOMO and LUMO orbitals, respectively [27], with the following relationships: $I = -E_{HOMO}$, $A = -E_{LUMO}$. The electronegativity ($\chi$) and chemical potential ($\mu$) are calculated using the relationships [28, 29]: $\chi = -\mu = (I + A)/2$. The value of the chemical potential ($\mu$) is –4.183 eV in the gaseous phase and –4.231 eV in the chloroform phase. Hardness is not observed physically, but this concept is used in chemistry and physics. In addition, soft molecules are large and highly polarized, whereas hard molecules are relatively small and much less polarized. Hardness ($\eta$) is equal to $\eta = (I - A)/2$ [28]. The softness ($\sigma$) of the investigated molecule is the inverse value of the hardness: $\sigma = 1/\eta$ [29]. In addition, hardness, softness, and electronegativity ($\chi$) values are very close for the gaseous and chloroform phases. All these values are given in Table 3.

*NMR spectra.* The BDBD compound was characterized using $^1$H and $^{13}$C NMR spectra. NMR spectra of the studied compound were measured in $CDCl_3$ solvent. Additionally, the NMR chemical shifts of the investigated series were

TABLE 1. Crystal Data, Collection, and Refinement Details

| Empirical formula | $C_{15}H_{16}BrNO_5$ |
|---|---|
| Formula weight | 370.20 |
| Temperature (K) | 100(0) |
| Wavelength (Å) | 0.71073 |
| Crystal system | Triclinic |
| Space group | *P*-1 |
| *a*, Å | 5.6744(3) |
| *b*, Å | 10.6569(6) |
| *c*, Å | 14.1753(8) |
| α, deg | 109.264(3) |
| β, deg | 90.670(3) |
| γ, deg | 104.941(3) |
| Volume, Å$^3$ | 777.44(8) |
| *Z* | 2 |
| Density (calculated), g/cm$^3$ | 1.581 |
| Absorption coefficient, mm$^{-1}$ | 2.666 |
| F(000) | 376 |
| Crystal size, mm | 0.050 × 0.100 × 0.800 |
| Crystal color | clear light white |
| θ range, degree | 3–27.62 |
| *h* | $-7 \le h \le 7$ |
| *k* | $-13 \le k \le 13$ |
| *l* | $-18 \le l \le 18$ |
| Reflection collected | 25857 |
| Independent reflections | 3603 [R(int) = 0.0391] |
| Data/restraints/parameters | 3603/0/201 |
| Absorption correction | multiscan |
| $T_{max}/T_{min}$ | 0.8780–0.2240 |
| Refinement method | Full-matrix least squares on $F^2$ |
| Final *R* indices [$I > 2\sigma(I)$] | $R_1 = 0.0253$, w$R_2 = 0.0598$ |
| *R* indices (all data) | $R_1 = 0.0327$, w$R_2 = 0.0631$ |
| Goodness-of-fit on $F^2$ | 1.054 |
| Largest diff. peak and hole, e/Å$^3$ | 0.404 and –0.278 |
| CCDC deposit number | 1976365 |

calculated with the GIAO method and the B3LYP functional 6-311G(*d*,*p*) basis set in the gaseous phase and chloroform solvent against the TMS standard. The experimental and theoretical NMR ($^1$H and $^{13}$C NMR) chemical shifts of the BDBD compound are presented in Table 4 as values relative to TMS.

TABLE 2. Experimental and Optimized Geometrical Parameters (bond lengths (Å), bond angles (degree), and dihedral angles (degree)) of BDBD

| Bond lengths | Experiment | B3LYP | | Bond angles | Experiment | B3LYP | | Dihedral angles | Experiment | B3LYP | |
|---|---|---|---|---|---|---|---|---|---|---|---|
| | | gas | solvent | | | gas | solvent | | | gas | solvent |
| Br1–C9 | 1.901(17) | 1.919 | 1.922 | N1–C6–C7 | 121.01(15) | 121.65 | 121.60 | O2–C4–C5–C11 | 92.70(16) | 91.39 | 91. 95 |
| O1–C3 | 1.454(2) | 1.440 | 1.443 | O1–C2–C1 | 111.78(15) | 110.17 | 110.97 | O2–N1–C6–C7 | –178.31(14) | 179.31 | 179.41 |
| O2–C4 | 1.449(2) | 1.455 | 1.459 | O2–C4–C3 | 108.33(14) | 108.97 | 109.33 | C11–C5–C6–N1 | –105.09(17) | –103.11 | –103.81 |
| O3–C11 | 1.445(2) | 1.446 | 1.444 | O3–C12–C13 | 111.82(15) | 110.94 | 111.09 | C11–C5–C6–C7 | 71.56(19) | 74.00 | 73.36 |
| C2–O5 | 1.192(2) | 1. 202 | 1. 207 | O4–C12–O3 | 122.97(16) | 123.42 | 123.16 | N1–C6–C7–C15 | –174.55(16) | –178.77 | –177.42 |
| C1–C2 | 1.497(2) | 1.506 | 1.505 | O5–C2–O1 | 123.30(16) | 124.06 | 124.07 | N1–C6–C7–C8 | 5.10(2) | 0.60 | 1.99 |
| C3–C4 | 1.506(2) | 1.515 | 1.511 | C11–C5–C4 | 115.88(13) | 116.29 | 116.60 | C15–C7–C8–C9 | 0.70(2) | –0.02 | –0.05 |
| C5–C11 | 1.532(2) | 1.538 | 1.539 | C14–C10–C9 | 118.28(15) | 118.58 | 118.47 | C7–C8–C9–C10 | –0.70(3) | –0. 01 | 0. 01 |
| C6–C7 | 1.476(2) | 1.470 | 1.471 | C14–C15–C7 | 120.11(16) | 120.12 | 120.22 | C8–C9–C10–C14 | 0.10(3) | –0.03 | –0.03 |
| C7–C8 | 1.401(2) | 1.406 | 1.406 | C15–C7–C8 | 119.57(15) | 119.29 | 119.24 | C12–O3–C11–C5 | 79.32(17) | 82.18 | 82.32 |
| C10–C14 | 1.386(3) | 1.391 | 1.391 | C2–O1–C3 | 117.41(14) | 117.58 | 116.15 | C4–C5–C11–O3 | 73.67(17) | 75.64 | 74.28 |
| C12–C13 | 1.496(2) | 1.506 | 1.504 | C6–C5–C4 | 98.56(13) | 98.16 | 98.32 | C11–O3–C12–C13 | –177.52(14) | 177.67 | 178.56 |
| C14–C15 | 1.393(2) | 1.393 | 1.393 | C6–N1–O2 | 108.83(14) | 110.08 | 110.06 | C10–C14–C15–C7 | –0.40(3) | –0.12 | –0.14 |
| O1–C2 | 1.342(2) | 1.361 | 1.352 | C7–C6–C5 | 125.05(15) | 125.69 | 125.63 | C6–C7–C15–C14 | 179.49(15) | 179.45 | 179.53 |
| N1–O2 | 1.418(18) | 1.390 | 1.394 | C8–C7–C6 | 119.77(15) | 119.82 | 119.98 | C3–O1–C2–O5 | 1.80(3) | –4.76 | –0.80 |
| O3–C12 | 1.350(2) | 1.356 | 1.355 | C8–C9–C10 | 122.58(16) | 121.75 | 121.91 | C2–O1–C3–C4 | –140.50(15) | –127.68 | –179.65 |
| C12–O4 | 1.206(2) | 1.206 | 1.209 | N1–C6–C5 | 113.86(14) | 112.60 | 112.71 | N1–O2–C4–C5 | 25.16(17) | 26.12 | 25.87 |
| N1–C6 | 1.285(2) | 1.285 | 1.285 | N1–O2–C4 | 107.85(12) | 108.02 | 107.93 | O1–C3–C4–C5 | –175.01(14) | –176.45 | –175.89 |
| C4–C5 | 1.534(2) | 1.536 | 1.537 | O1–C3–C4 | 106.85(14) | 107.79 | 106.59 | C3–C4–C5–C6 | –143.34(15) | –146.23 | –146.29 |
| C5–C6 | 1.513(2) | 1.524 | 1.523 | O1–C3–H5 | 110.40 | 109.22 | 109.41 | C3–C4–C5–C11 | –26.90(2) | –29.45 | –29.21 |
| C7–C15 | 1.398(2) | 1.402 | 1.402 | O2–C4–C5 | 104.23(13) | 103.61 | 103.60 | O2–N1–C6–C5 | –1.50(2) | –3.45 | –3.28 |
| C8–C9 | 1.380(2) | 1.384 | 1.384 | O3–C11–C5 | 111.05(13) | 111.82 | 111.65 | C4–C5–C6–N1 | 16.27(18) | 18.66 | 18.42 |
| C9–C10 | 1.388(2) | 1.395 | 1.394 | O3–C11–H9 | 109.40 | 108.88 | 108.97 | C4–C5–C6–C7 | –167.08(15) | –164.23 | –164.41 |
| | | | | O4–C12–C13 | 125.21(16) | 125.63 | 125.75 | C5–C6–C7–C15 | 9.00(3) | 4.36 | 5.64 |
| Bond angles | | | | O5–C2–C1 | 124.92(16) | 125.77 | 125.97 | C5–C6–C7–C8 | –171.28(15) | –176.27 | –174.94 |
| C10–C14–C15 | 120.68(16) | 120.83 | 120.80 | | | | | C6–C7–C8–C9 | –178.97(15) | –179.40 | –179.47 |
| C10–C9–Br1 | 119.39(13) | 119.08 | 119.04 | Dihedral angles | | | | C7–C8–C9–Br1 | 178.36(12) | 179.97 | –179.97 |
| C12–O3–C11 | 115.11(13) | 116.39 | 116.67 | C4–O2–N1–C6 | –15.44(19) | –14.90 | –14.84 | Br1–C9–C10–C14 | –178.92(13) | 179.99 | 179.94 |
| C15–C7–C6 | 120.66(15) | 120.89 | 119.24 | C3–O1–C2–C1 | –178.33(16) | 174.95 | 179.17 | C6–C5–C11–O3 | –176.13(12) | –174.19 | –175.13 |
| C3–C4–C5 | 117.14(14) | 118.55 | 118.35 | N1–O2–C4–C3 | 150.60(14) | 153.22 | 152.93 | C11–O3–C12–O4 | 2.30(2) | –2.40 | –1.74 |
| C6–C5–C11 | 109.31(13) | 109.70 | 109.75 | O1–C3–C4–O2 | 67.55(17) | 65.50 | 65.92 | C9–C10–C14–C15 | 0.40(3) | 0.10 | –0.10 |
| C8–C9–Br1 | 118.02(13) | 119.17 | 119.05 | O2–C4–C5–C6 | –23.70(15) | –25.39 | –25.13 | C8–C7–C15–C14 | –0.20(3) | 0.08 | 0.11 |

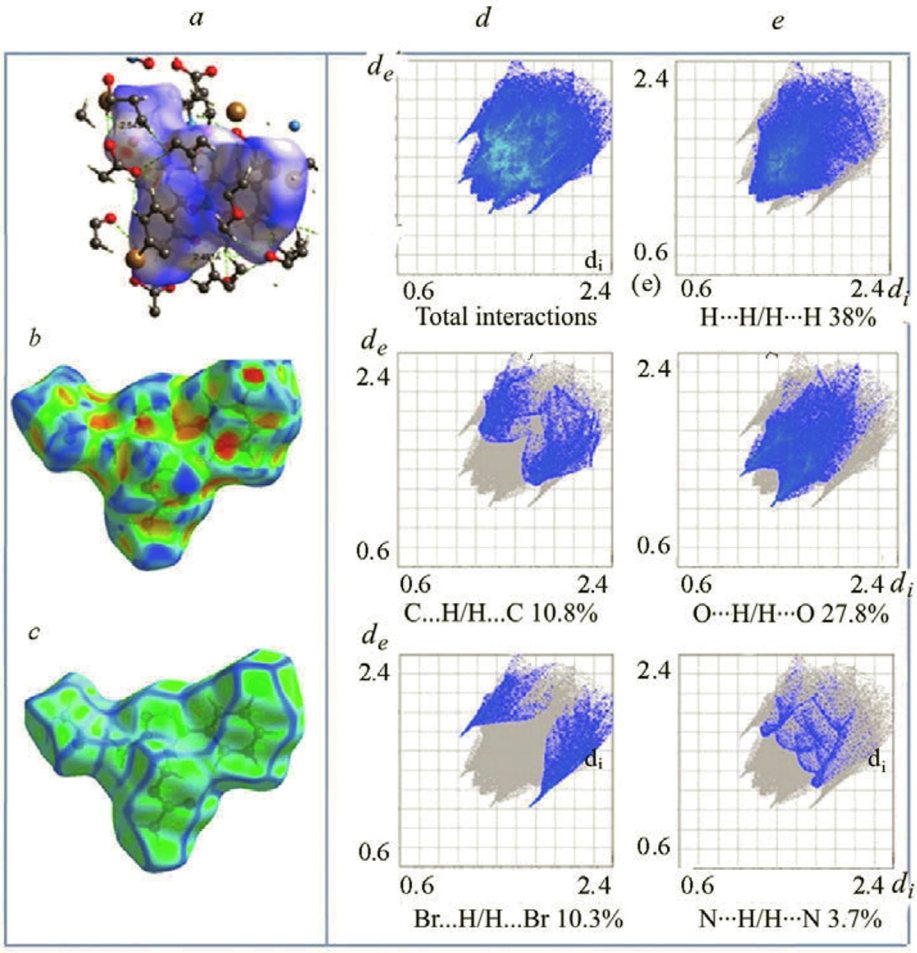


Fig. 2. Hirschfeld surface with (a) $d_{norm}$, (b) shape index, (c) curvedness, and 2D fingerprint plots (d) full, (e) H···H, (f) C···H/H···C, (g) O···H/H···O, (h) Br···H/H···Br, and (i) N···H/H···N contacts contributing to the Hirschfeld surface area of BDBD.

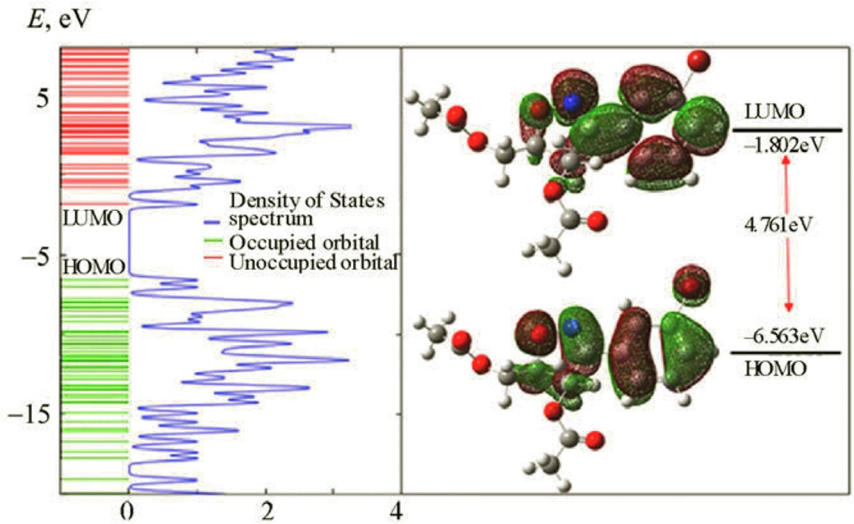


Fig. 3. The 3D orbital pictures of the HOMO, LUMO, and DOS diagrams calculated at the B3LYP/6-311G(*d*,*p*) level in the gaseous phase for the BDBD molecule.

TABLE 3. Total Energy, $E_{HOMO}$, $E_{LUMO}$, $\Delta E_{HOMO\text{-}LUMO}$ Values, Ionization Potential ($I$), Electron Affinity ($A$), Electronegativity (χ), Hardness (η), Softness (σ), and Chemical Potential (μ) of BDBD

| Parameter | Gas phase | Chloroform phase |
|---|---|---|
| Total energy, eV | –97593.249 | –97593.546 |
| $E_{HOMO}$, eV | –6.563 | –6.614 |
| $E_{LUMO}$, eV | –1.802 | –1.847 |
| $\Delta E_{HOMO–LUMO}$, eV | 4.761 | 4.767 |
| $I$, eV | 6.563 | 6.614 |
| $A$, eV | 1.802 | 1.847 |
| χ, eV | 4.183 | 4.231 |
| η, eV | 2.381 | 2.384 |
| σ, $eV^{-1}$ | 0.420 | 0.419 |
| μ, eV | –4.183 | –4.231 |

TABLE 4. $^{1}H$ and $^{13}C$ Chemical Shifts (ppm) (with respect to TMS) for the BDBD Compound

| H | Experiment | GIAO | C | Experiment | GIAO |
|---|---|---|---|---|---|
| H14 | 7.91 | 8.32 | C12 | 170.56 | 174.86 |
| H12 | 7.67 | 7.87 | C2 | 170.44 | 171.99 |
| H13 | 7.57 | 7.37 | C6 | 156.73 | 160.01 |
| H2 | 7.30 | 7.32 | C9 | 133.49 | 146.80 |
| H5 | 4.86 | 5.72 | C10 | 130.52 | 137.10 |
| H15 | 4.64 | 4.58 | C7 | 130.22 | 135.41 |
| H10 | 4.45 | 4.40 | C14 | 129.96 | 133.43 |
| H4 | 4.34 | 3.78 | C8 | 125.55 | 133.38 |
| H9 | 4.17 | 3.63 | C15 | 123.08 | 129.59 |
| H11 | 3.95 | 3.39 | C4 | 81.37 | 86.74 |
| H7 | 2.14 | 2.20 | C3 | 61.32 | 62.34 |
| H6 | 2.14 | 2.05 | C11 | 59.26 | 62.00 |
| H8 | 2.14 | 1.96 | C5 | 47.79 | 51.07 |
| H3 | 2.04 | 1.95 | C13 | 20.80 | 20.54 |
| H16 | 2.04 | 1.67 | C1 | 20.71 | 20.39 |
| H1 | 2.04 | 1.65 | | | |
| Correlation coefficient $R^2 = 0.9892$ | | | Correlation coefficient $R^2 = 0.9983$ | | |

The $^{1}H$ NMR spectrum of the BDBD compound shows four types of hydrogen atoms (protons): aromatic, methyl ($–CH_3$), methylene ($–CH_2$), and methine (–CH). In the experimental $^{1}H$ NMR spectrum of the BDBD compound, aromatic protons appeared in the range 7.30–7.91 ppm. Their theoretical values were calculated to be between 7.32 and 8.32 ppm (Table 4). Methyl groups ($–CH_3$) appeared at 2.14 (H6, H7, and H8) and 2.04 (H1, H3, and H16) ppm in the experimental

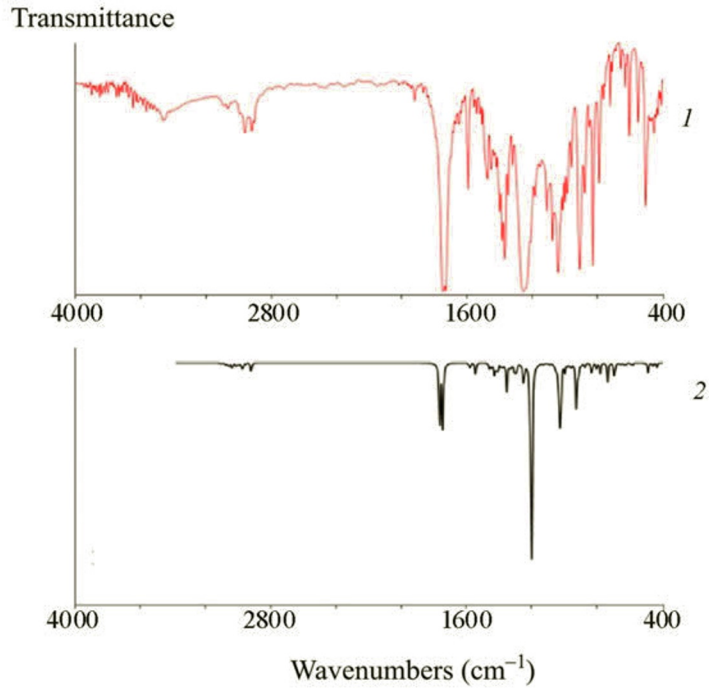


Fig. 4. The experimental (1) and calculated (2) FT-IR spectra in the range of 4000–400 cm$^{-1}$ of BDBD.

$^{1}$H NMR spectrum. In the theoretical spectrum, these signals were calculated at 2.20 (H7), 2.05 (H6), 1.96 (H8), 1.95 (H3), 1.67 (H16), and 1.65 (H1) ppm, respectively.

The $^{1}$H NMR spectrum of the studied molecule has two separate peaks of methylene (–$CH_2$) groups in each of the diacetate chains. Experimentally, in the $^{1}$H NMR spectrum of the studied compound, methylene protons appeared in the C5-linked acetate chain of the isoxazole ring at 4.17 and 4.45 ppm (3.63 and 4.40 ppm theoretically), while the other methylene protons were observed at 4.34 ppm (3.78 ppm theoretically) and 4.86 (5.72 ppm theoretically). They were reported at 4.48 and 4.79 ppm in the $^{1}$H NMR spectrum for 10-benzoyloxy-8,9-epoxy-6-methoxymethyl isobutyrate, which is derived from acetate [30].

The chemical shift of the –C5H11 proton (methine proton) occurred at 3.95 ppm in the experimental $^{1}$H NMR spectrum and 3.39 ppm in the predicted $^{1}$H NMR spectrum. The experimental and theoretical chemical shift values of the other methine proton (–C4H15) were 4.58 and 4.64 ppm, respectively. The correlation between the experimental and calculated $^{1}$H NMR chemical shifts was satisfactory ($R^2$ = 0.9892).

In the 13C NMR spectrum of the BDBD compound, nine peaks other than aromatic carbons were observed, which was in agreement with the molecular structure. These were two carbonyl carbons (C=O), an azomethine carbon (C=N), two methyl carbons (–CH3), two methylene carbons (–CH2), two methine carbons (–CH), and six aromatic carbons. Carbons C2 and C12 of carbonyl (C=O) were observed at 170.56 and 170.44 ppm (calculated as 171.99 and 174.86 ppm). The signal of an azomethine (C=N) was observed at 156.73 ppm (calculated as 160.01 ppm), which agrees with the value reported in an earlier study of 156.90 ppm for 5-(nitromethyl)-3-phenyl-4,5-dihydroisoxazole [31].

The aromatic carbon signals were between 123.08 and 133.49 ppm in the experimental $^{13}$C NMR spectrum (129.59–146.80 ppm calculated values). The resonances in the experimental $^{13}$C NMR spectrum at 81.37 and 47.79 ppm correspond to methine carbons (C4 and C5), respectively (with theoretical chemical shift values of 86.74 and 51.07 ppm). In the $^{13}$C NMR spectrum, methylene carbon (–$CH_2$) resonances were found experimentally at 59.26 and 61.32 ppm and calculated at 62.00 and 62.34 ppm, respectively. In the experimental $^{13}$C NMR spectrum of the studied compound, methyl (–$CH_3$) carbons appeared at 20.80 (calculated as 20.54 ppm) and 20.71 ppm (calculated as 20.39 ppm). The correlation coefficients for the dependences of the calculated chemical shifts on the experimental values were larger than 0.99 (see Table 4; $R^2$= 0.9983), indicating excellent correlation.

*Vibrational frequencies.* Some characteristic FT-IR assignments of BDBD determined by the DFT/B3LYP/6-311G(*d*,*p*) method, along with the potential energy distribution (PED) contributions, are shown in Table 5 in comparison

TABLE 5. Comparison of the Experimental and Theoretical Vibrational Frequencies ($cm^{-1}$) by the B3LYP with the 6-311G(*d*,*p*) Basis Set

| *v* | Assignments (%PED[a]) | Experiment | B3LYP | | *v* | Assignments (%PED[a]) | Experiment | B3LYP | |
|---|---|---|---|---|---|---|---|---|---|
| | | | Unscaled | Scaled | | | | Unscaled | Scaled |
| 1 | $\nu_s(CH)_{ph}(99)$ | 3452 | 3217 | 3111 | 40 | $\sigma(HCO3)(41)$, $\tau(HCCC)_{iso}(15)$ | – | 1289 | 1246 |
| 2 | $\nu_s(CH)_{ph}(86)$ | 3096 | 3207 | 3101 | 41 | $\nu(O3C)(22)$, $\nu(CC)(14)$, $\sigma(O4CC)(14)$ | 1211 | 1246 | 1205 |
| 3 | $\nu_s(CH)_{ph}(91)$ | 3082 | 3192 | 3087 | 42 | $\beta(HCC)_{iso}(59)$ | – | 1241 | 1200 |
| 4 | $\nu_{as}(C13H_3)(94)$ | 3069 | 3161 | 3057 | 43 | $\nu(O1C)(22)$, $\nu(CC)(12)$, $\sigma(O5CC)(12)$ | 1184 | 1237 | 1196 |
| 5 | $\nu_{as}(C1H_3)(94)$ | 3061 | 3159 | 3055 | 44 | $\sigma(HCC)_{ph}(69)$ | 1153 | 1203 | 1163 |
| 6 | $\nu_{as}(C3H_2)(13)$, $\nu_{as}(C11H_2)(82)$ | 3040 | 3145 | 3041 | 45 | $\nu(CC)(25)_{iso}$ | 1136 | 1165 | 1127 |
| 7 | $\nu_{as}(C3H_2)(83)$, $\nu_{as}(C11H_2)(10)$ | – | 3137 | 3033 | 46 | $\nu(CC)_{iso}(30)$ | 1101 | 1126 | 1089 |
| 8 | $\nu_{as}(C1H_3)(98)$ | – | 3114 | 3011 | 47 | $\nu(CC)_{iso}(10)$, $\sigma(HCC)_{ph}(20)$, $\nu(CC)_{ph}(24)$ | 1076 | 1123 | 1086 |
| 9 | $\nu_{as}(C13H_3)(99)$ | – | 3113 | 3010 | 48 | $\sigma(HCC)_{ph}(17)$, $\nu(CC)_{ph}(39)$ | – | 1094 | 1058 |
| 10 | $\nu_s(C5H)_{iso}(88)$ | 2993 | 3103 | 3001 | 49 | $\nu(CC)(22)_{iso}$ | 1041 | 1080 | 1044 |
| 11 | $\nu_s(C11H_2)(90)$ | | 3089 | 2987 | 50 | $\tau(O5CO1C)(19)$, $\tau(O4CO3C)(18)$, $\tau(HCCO1)(45)$ | – | 1066 | 1030 |
| 12 | $\nu_s(C3H_2)(99)$ | 2962 | 3073 | 2972 | 51 | $\tau(HCCO3)(31)$, $\nu(O1C)(31)$ | – | 1062 | 1027 |
| 13 | $\nu_s(C13H_3)(99)$ | 2937 | 3052 | 2951 | 52 | $\nu(CC)_{iso}(14)$ | – | 1061 | 1026 |
| 14 | $\nu_s(C1H_3)(100)$ | – | 3051 | 2950 | 53 | $\nu(O3C)(31)$ | 1013 | 1053 | 1018 |
| 15 | $\nu_s(C4H)_{iso}(99)$ | 2920 | 3018 | 2918 | 54 | $\tau(HCCC)_{iso}(11)$ | 1001 | 1028 | 994 |
| 16 | $\nu(C2{=}O5)(87)$ | 1745 | 1822 | 1762 | 55 | $\beta(CCC)_{ph}(59)$ | 987 | 1010 | 977 |
| 17 | $\nu(C12{=}O4)(87)$ | 1730 | 1802 | 1743 | 56 | $\tau(CCCC)_{ph}(25)$, $\tau(HCCC)_{iso}(60)$ | 960 | 1001 | 968 |
| 18 | $\nu(C{=}N)(60)$ | 1591 | 1640 | 1586 | 57 | $\nu(O1C)(11)$, $\nu(O3C)(14)$ | – | 985 | 952 |
| 19 | $\nu(CC)_{ph}(46)$ | 1570 | 1631 | 1577 | 58 | $\nu(O2N)_{iso}(43)$ | – | 957 | 925 |
| 20 | $\nu(CC)_{ph}(48)$, $\nu(C{=}N)(14)$ | 1541 | 1594 | 1541 | 59 | $\nu(O2N)_{iso}(22)$, $\sigma(CO2N)_{iso}(10)$ | – | 944 | 913 |
| 21 | $\rho(HCC)_{ph}(49)$, $\nu(CC)_{ph}(14)$ | 1474 | 1507 | 1457 | 60 | $\tau(HCCC)_{ph}(71)$ | 908 | 938 | 907 |
| 22 | $\sigma(C11H_2)(27)$, $\sigma(C3H_2)(58)$ | 1454 | 1495 | 1446 | 61 | $\tau(HCCC)_{ph}(58)$ | – | 922 | 892 |
| 23 | $\sigma(C11H_2)(47)$, $\sigma(C3H_2)(30)$ | 1435 | 1491 | 1442 | 62 | $\nu(O2C)_{iso}(20)$ | 878 | 902 | 872 |
| 24 | $\sigma(C1H_3)(77)$ | 1420 | 1477 | 1428 | 63 | $\nu(O3C)(23)$, $\nu(O1C)(11)$, $\nu(CC)_{iso}(14)$ | 851 | 859 | 831 |
| 25 | $\sigma(C13H_3)(77)$ | – | 1476 | 1427 | 64 | $\nu(O3C)(13)$, $\nu(O1C)(19)$ | 827 | 852 | 824 |
| 26 | $\sigma(C1H_3)(77)$ | – | 1473 | 1424 | 65 | $\nu(CC)_{iso}(15)$, $\nu(O2C)_{iso}(27)$ | 791 | 828 | 801 |
| 27 | $\sigma(C13H_3)(76)$ | – | 1471 | 1422 | 66 | $\tau(HCCC)_{ph}(66)$ | 764 | 805 | 778 |
| 28 | $\nu(CC)_{ph}(37)$, $\sigma(HCC)(17)$ | 1398 | 1456 | 1408 | 67 | $\nu(O2C)_{iso}(12)$, $\sigma(CO2N)_{iso}(17)$ | 721 | 756 | 731 |
| 29 | $\tau(HCO1C)(42)$, $\tau(HCO2N)(20)$ | 1385 | 1432 | 1388 | 68 | $\beta(CCC)_{ph}(10)$, $\sigma(CCO2)_{iso}(14)$ | 689 | 714 | 690 |
| 30 | $\tau(HCO3C)(57)$ | 1369 | 1417 | 1370 | 69 | $\nu(CC)(18)$, $\sigma(CCO3)(10)$ | 658 | 679 | 657 |
| 31 | $\rho(C13H_3)(78)$ | 1348 | 1398 | 1352 | 70 | $\beta(CCC)_{ph}(67)$ | 640 | 665 | 643 |
| 32 | $\rho(C1H_3)(77)$ | | 1396 | 1350 | 71 | $\beta(CO1C)(22)$, $\nu(CC)(31)$ | 631 | 653 | 631 |
| 33 | $\sigma(HCO1)(10)$, $\sigma(HCO2)(38)$ | | 1375 | 1330 | 72 | $\tau(CCNC)(16)$ | | 640 | 619 |
| 34 | $\sigma(HCO2)(21)$, $\sigma(HCO3)(18)$ | 1321 | 1365 | 1320 | 73 | $\tau(O4CO3C)(51)$ | 602 | 609 | 589 |
| 35 | $\nu(C6C7)(15)$, $\nu(CC)_{iso}(12)$, $\sigma(HCC)_{ph}(23)$ | | 1350 | 1306 | 74 | $\tau(O5CO1C)(59)$ | 552 | 598 | 578 |
| 36 | $\tau(HCO2N)(28)$ | | 1337 | 1293 | 75 | $\tau(BrCCC)(21)$ | 505 | 526 | 509 |
| 37 | $\tau(HCO2N)(11)$, $\sigma(HCC)_{ph}(23)$ | | 1336 | 1292 | 76 | $\sigma(CCN)_{iso}(10)$, $\sigma(CCO2)(17)$ | 480 | 499 | 483 |
| 38 | $\nu(CC)_{ph}(53)$, $\sigma(HCC)_{ph}(19)$ | | 1304 | 1261 | 77 | $\sigma(O5CC)(17)$, $\sigma(O4CC)(11)$ | 453 | 469 | 454 |
| 39 | $\sigma(HCO1)(46)$, $\sigma(HCO2)(15)$ | 1252 | 1292 | 1249 | 78 | $\tau(CCCC)_{ph}(53)$, $\sigma(O4CC)(27)$ | 430 | 445 | 430 |

Note. Potential energy distribution (PED) ≤ 10% are not shown; ν, stretching; β, in-plane bending; γ, out-of-plane bending; τ, torsion; σ, scissoring; ρ, rocking; s, symmetric; as, antisymmetric; ph, phenyl; iso, isoxazole.

with the experimental results. The frequencies obtained from the B3LYP calculation were scaled by a factor of 0.967, which is a typical correction factor for the B3LYP frequencies [32]. The measured and calculated FT-IR spectra in the range 4000–400 $cm^{-1}$ of BDBD are presented in Fig. 4.

*C–H vibrations of the phenyl ring.* The C–H vibrations of the phenyl ring appeared at higher frequencies than the C–H vibrations of the isoxazole ring. In the aromatic ring, the C–H stretching vibrations appear in the range 3100–3000 $cm^{-1}$ [33]. The FT-IR bands at 3452, 3096, and 3082 $cm^{-1}$ assigned to the ν(C–H) stretching vibrations of the phenyl ring. These peaks were calculated at 3111, 3101, and 3087 $cm^{-1}$ for the B3LYP level of theory with 99, 86, and 91% contributions to the PED, respectively. The C–H in-plane bending vibrations and the C–H out-of-plane bending vibrations normally appear in the 1100–1500 and 750–1000 $cm^{-1}$ frequency region, respectively [34].

The C–H in-plane bending vibration modes [$\rho(HCC)_{ph}$], which contributed to 17–69% of PED, were calculated in the range 1058–1457 $cm^{-1}$ for the B3LYP level. The $\rho(HCC)_{ph}$ vibration modes (ν21, ν35, ν37, ν38, ν44, and ν48) were observed at 1474 and 1153 $cm^{-1}$ in the FT-IR spectrum, experimentally. The C–H out-of-plane bending vibration modes [$\tau(HCCC)_{ph}$] of the phenyl ring were responsible for the peaks at 908, and 764 $cm^{-1}$ in the FT-IR spectrum. The $\tau(HCCC)_{ph}$ vibration modes were assigned at 907, 892, and 778 $cm^{-1}$ with 71, 58, and 66% contributions to PED, respectively.

*Methyl (–$CH_3$) and methylene (–$CH_2$) groups modes.* The asymmetric and symmetric stretching vibrations of the methyl (–$CH_3$) group are expected in the range 2900–3050 $cm^{-1}$ [35]. The wavenumbers of asymmetric stretching vibrations are generally higher than symmetric ones. Asymmetric stretching vibrations [$\nu_{as}(C13H_3)$ and $\nu_{as}(C1H_3)$] for the presence of methyl groups were observed in the FT-IR spectrum at 3069 and 3061 $cm^{-1}$ experimentally; theoretically, quite pure modes were found at 3057, 3010 $cm^{-1}$ and 3055, 3011 $cm^{-1}$, contributing to >94% of PED. Meanwhile, symmetric stretching vibrations [$\nu_s(C13H_3)$ and $\nu_s(C1H_3)$] in the presence of methyl groups were observed at 2937 $cm^{-1}$ in the FT-IR spectrum with theoretical values of 2951 and 2950 $cm^{-1}$ in the B3LYP/6-311G(*d*,*p*) level of the theory with almost ~100% contribution to PED. The $\sigma(C1H_3)$ and $\sigma(C13H_3)$ bending vibrations of the methyl groups should appear between 1410 and 1550 $cm^{-1}$ [36]. The $\sigma(C1H_3)/\rho(C1H_3)$ and $\sigma(C13H_3)/\rho(C13H_3)$ bending vibrations of the methyl groups were observed at 1420/1348 $cm^{-1}$ for BDBD, while the DFT/B3LYP/6-311G(*d*,*p*) calculation gives the $\sigma(C1H_3)/\rho(C1H_3)$ and $\sigma(C13H_3)/\rho(C13H_3)$ bending vibrations at 1428, 1424/1350 $cm^{-1}$ (77% PEDs) and 1427, 1422/1352 $cm^{-1}$ (~78% PED). The out-of-plane τ(HCCO1) and τ(HCCO3) bending vibration modes (ν50 and ν51) of the methyl group were computed at 1030 and 1027 $cm^{-1}$ with 45% and 31% contributions to PED, respectively.

The asymmetric $\nu\nu_{as}(CH_2)$ stretching vibration was generally observed in the range 2900–3000 $cm^{-1}$, while the $\nu_s(CH_2)$ symmetric stretching vibrations appeared between 2800 and 2900 $cm^{-1}$ [37]. The shoulder located at 3040 $cm^{-1}$ in the FT-IR spectrum of BDBD was assigned to the $\nu_{as}(C11H_2)$ and $\nu_{as}(C3H_2)$ asymmetric stretching modes of the methylene ($CH_2$) groups, and the intense band at 2962 $cm^{-1}$ in the FT-IR spectrum should be due to the $\nu_s(C11H_2)$ and $\nu_s(C3H_2)$ symmetric stretching modes. The $\nu_{as}(C11H_2)$, $\nu_{as}(C3H_2)$ and $\nu_s(C11H_2)$, $\nu_s(C3H_2)$ were computed at 3041, 3033 and 2987, 2972 $cm^{-1}$ (mode *ν*6, *ν*7 and *ν*11, *ν*12) with 82, 83 and 90, 99% PEDs, respectively. For BDBD, the bending peaks of $\sigma(C3H_2)$ and $\sigma(C11H_2)$ were 1454 and 1435 $cm^{-1}$, while the DFT calculation gives the bending vibrations $\sigma(C3H_2)$ and $\sigma(C11H_2)$ as 1446 and 1442 $cm^{-1}$, respectively.

*C=O and C-O vibrations.* The C=O carbonyl band appears to be very sensitive to various factors such as the physical state, electronic effects by substituents, and ring strains [38, 39]. The C=O carbonyl vibrational bands had a somewhat decreased influence due to substitutions of methyl groups. The title compound showed sharp intense absorption bands at 1745 and 1730 $cm^{-1}$ due to the carbonyl ν(C2=O5) and ν(C12=O4) groups of the acetate chains. The theoretical values were 1762 and 1743 $cm^{-1}$ (DFT/B3LYP) with 87% contribution to PED. These modes are 16 and 17, which belong to the C=O stretching vibrations of both acetate chains. The τ(O4CO3C) and τ(O5CO1C)/σ(O4CC) and σ(O5CC) out-of-plane/in-plane bending vibration bands of the acetate chains were observed at 602 and 552/453 $cm^{-1}$ in the FT-IR spectrum and appeared at 589 and 578/454 $cm^{-1}$ in the theoretical spectrum for the B3LYP/6-311G(*d*,*p*) level of theory. According to the calculated PED distributions using the B3LYP/6-311G(*d*,*p*) level of theory, the participation of the C=O modes in these vibrations was 51 and 59/11% and 17%.

The theoretical values of the $\nu(O2C)_{iso}$/ν(O3C) and ν(O1C) stretching vibrations for the isoxazole ring/acetate chains were calculated at 872, 801 $cm^{-1}$/1205, 1018, and 952 $cm^{-1}$ and at 1196, 1027, and 952 $cm^{-1}$ using the B3LYP/6-311G(*d*,*p*) level of the theory with PED contributions of 20, 27/22, 31, and 14% as well as 2, 31, and 11%, respectively. The $\nu(O2C)_{iso}$/ν(O3C) and ν(O1C) stretching vibrations on the isoxazole ring/acetate chains appeared at 878 and 791/1211 and 1013 $cm^{-1}$ as well as 1184 $cm^{-1}$ experimentally, respectively. The $\sigma(HCO2)_{iso}$, σ(HCO1), and σ(HCO3) in-plane bending modes (ν34, ν34, ν39, ν40) were assigned the frequencies 1330–1246 (10–46%) $cm^{-1}$ on the isoxazole ring and acetate

chains. The corresponding $\sigma(HCO2)_{iso}$, σ(HCO1), and σ(HCO3) in-plane bending modes were observed at 1321 and 1252 $cm^{-1}$ in the FT-IR spectrum.

*C–C, C=N, and N–O vibrations.* The stretching vibrations of ν(C–C) in the phenyl ring and of ν(C=N) in the isoxazole ring were recorded at 1430–1650 $cm^{-1}$ and 1580–1675 $cm^{-1}$, respectively [40, 41]. The experimental and computed values of these bands were at 1570, 1541, and 1577 (46%), 1541 (48%) /1591, and 1586 (60%) $cm^{-1}$ at the B3LYP/6-311G(*d*,*p*) level of the theory in the FT-IR spectrum for BDBD, respectively. According to [42], the C-C stretching band in the aromatic ring and the C=N stretching band in the isoxazole moiety were at 1592 and 1586 $cm^{-1}$, respectively. The N–O stretching vibration modes were assigned at 910.4 $cm^{-1}$ experimentally and between 912.6–923.2 $cm^{-1}$ theoretically, while these appeared at 977 $cm^{-1}$ for 6-31G+(*d*,*p*) [43], at 949 $cm^{-1}$ for 6-31G (*d*,*p*), and at 948 $cm^{-1}$ for 6-311+G(*d*,*p*) [42], with basis sets in isoxazole moiety. The computed peaks at 925 and 913 $cm^{-1}$ accounted for 43 and 22% of PEDs in the B3LYP/6-311G(*d*,*p*) level of the theory due to the $\nu(O2N)_{iso}$ stretching modes of BDBD.

The experimental absorption peaks at 987 and 640 cm–1 (977 and 643 $cm^{-1}$ for the B3LYP/6-311G(d,p) level of the theory) in the FT-IR spectrum were assigned to the β(CCC)ph in-plane bending modes of the phenyl ring for BDBD. The corresponding out-of-plane bending modes $\tau(CCCC)_{ph}$ were observed at 1321 and 1252 $cm^{-1}$ in the FT-IR spectrum. The $\sigma(CO2N)_{iso}$ and $\sigma(CCN)_{iso}$ in-plane bending modes (ν67 and ν76) were assigned the frequencies 721 and 480 $cm^{-1}$ in the FT-IR spectrum/731 (17%) and 483 (10%) $cm^{-1}$ using the B3LYP/6-311G(*d*,*p*) level on the isoxazole ring, respectively.

**Conclusions.** The crystal structure of the BDBD compound was determined using single crystal X-ray diffraction analysis, which is reported here for the first time. The BDBD compound exists in triclinic crystal packing with space group P-1 in the solid state. Hirschfeld surface analysis and FPs were applied to confirm the existence of strong C=O···H interactions in the crystal. Analysis of the calculated geometry parameters using the DFT/B3LYP method with the 6-311G(*d*,*p*) basis set and comparison with single crystal XRD data are very helpful in determining the unambiguous locations of atoms as well as the most stable geometry. The $E_{HOMO}$ and $E_{LUMO}$ values for the BDBD molecule were –6.563 eV and –1.802 eV, respectively, whereas the energy gap ($\Delta E$) was 4.761 eV for the gaseous phase. The theoretical $^{1}H$ and $^{13}C$ NMR spectra were found to be compatible with the experimental ones. FT-IR spectrum characterization was performed both experimentally and theoretically.

## REFERENCES


1. I. Zadrozna, J. Kurkowska, H. Kruszewska, and I. Makuch, *Farmaco*, **55**, 499–501 (2000).
2. M. Shailaja, A. Manjula, and B. V. Rao, *Indian J. Chem.*, **50B**, 214–222 (2011).
3. J. T. Pulkkinen, P. Honkakoski, M. Perakyla, I. Berczi, and R. Laatikainen, *J. Med. Chem.*, **51**, 3562–3571 (2008).
4. C. T. Molina and A. A. de Palermo, *Heterocycl. Commun.*, **9**, 535–538 (2011).
5. P. Mondal, S. Jana, A. Balaji, R. Ramakrishna, and K. L. Kanthal, *J. Young Pharm.*, **4**, 38–41 (2012).
6. Y. S. Kara, *Spectrochim. Acta A*, **151**, 723–730 (2015).
7. G. M. Sheldrick, *Acta Crystallogr. C: Struct. Chem.*, **71**, 3–8 (2015).
8. G. M. Sheldrick, *Acta Crystallogr. A*, **64**, 112–122 (2008).
9. Bruker, SHELXTL, Bruker AXS Inc., Madison, Wisconsin, USA (2006).
10. A. L. Spek, *PLATON-a Multipurpose Crystallographic Tool*, Utrecht University (2005).
11. L. Farrugia, *J. Appl. Crystallogr.*, **45**, 849–854 (2012).
12. O. V. Dolomanov, L. J. Bourhis, R. J. Gildea, J. A. K. Howard, and H. Puschmann, *J. Appl. Crystallogr.*, **42**, 339–341 (2009).
13. *Gaussian 09, Revision A.1*, Gaussian Inc., Wallingford CT, 2009.
14. T. Keith and J. Millam, GaussView, Version 5.0.9, Semichem. Inc., Shawnee Mission, KS (2009).
15. A. D. Becke, *J. Chem. Phys.*, **98**, 5648–5652 (1993).
16. C. Lee, W. Yang, and R. G. Parr, *Phys. Rev. B*, **37**, 785–789 (1988).
17. E. Cances, B. Mennucci, and J. Tomasi, *J. Chem. Phys.,* **107**, 3032–3041 (1997).
18. N. M. O'Boyle, A. L. Tenderholt, and K. M. Langner, *J. Comput. Chem.*, **29**, 839 (2008).
19. M. N. Arshad, Al-Anood M. Al-Dies, A. M. Asiri, M. Khalid, A. S. Birinji, K. A. Al-Amry, and A. A. C. Braga, *J. Mol. Struct.*, **1141**, 142–156 (2017).
20. D. E. Taylor and R. C. Sausa, *J. Mol. Struct.,* **1162**, 45–53 (2018).
21. N. Dege, N. Senyüz, H. Batı, N. Günay, D. Avcı, O. Tamer, and Y. Atalay, *Spectrochim. Acta A*, **120**, 323–331 (2014).
22. H. L. Hirshfeld, *Theor. Chim. Acta*, **44**, 129–138 (1977).

23. M. J. Turner, J. J. McKinnon, S. K. Wolff, D. J. Grimwood, P. R. Spackman, D. Jayatilaka, and M. A. Spackman, *Crystal Explorer*, The University of Western Australia (2017).
24. S. H. Sumrra, A. H. Atif, and M.N. Zafar, *J. Mol. Struct.,* **1166**, 110–120 (2018).
25. N. M. O'Boyle, A. L. Tenderholt, and K. M. Langner, *J. Comput. Chem*., **29**, 839 (2008).
26. S. M. Hiremath, A. S. Patil, C. S. Hiremath, M. Basangoudac, S. S. Khemalapure, N. R. Patil, S. B. Radder, S. J. Armakovi, and S. Armakovi, *J. Mol. Struct.*, **1178**, 1–17 (2019).
27. C. Zhan, J. A. Nichols, and D. A. Dixon, *J. Phys. Chem. A*, **107**, 4184–4195 (2003).
28. P. Govindasamy and S. Gunasekaran, *Spectrochim. Acta A*, **149**, 800–811 (2015).
29. A. Lesar and I. Milosev, *Chem. Phys. Lett.*, **483**, 198–203 (2009).
30. C. Bustos-Brito, V. J. Vázquez-Heredia, F. Calzada, L. Yépez-Mulia, J. S. Calderón, S. Hernández-Ortega, B. Esquivel, N. García-Hernández, and L. Quijano, *Molecules*, **21**, 1132–1144 (2016).
31. B. Mirosław, D. Babyuk, A. Łapczuk-Krygier, A. Kacka-Zych, O. M. Demchuk, and R. Jasin'ski, *Monatsh. Chem. Chem. Mon.*, **149**, 1877–1884 (2018).
32. A. Esme and S. G. Sagdinc, *J. Mol. Struct.,* **1048**, 185–195 (2013).
33. G. Varsanyi, L. Lang, and M.A. Kovner, *Assignments for Vibrational Spectra of Seven Hundred Benzene Derivatives*, Academiai Kiado, Budapest, **44**, 22 (1973).
34. S. Muthu and J. U. Maheswari, *Spectrochim. Acta A*, **92**, 154–163 (2012).
35. N. B. Colthup, L. H. Daly, and S. E. Wiberly, *Introduction to Infrared and Raman Spectroscopy*, Academic Press, New York (1975).
36. M. Diem, *Introduction to Modern Vibrational Spectroscopy*, Wiley, New York (1993).
37. D. Sajan, J. Binoy, B. Pradeep, K. V. Krishnan, V. B. Kartha, I. H. Joe, and V. S. Jayakumar, *Spectrochim. Acta A*, **60**, 173–180 (2004).
38. D. N. Sathyanarayana, *Vibrational Spectroscopy — Theory and Applications*, New Age International (P) Ltd. Publishers, New Delhi (2004).
39. M. E. D. Lestard, M. E. Tuttolomondo, D. A. Wann, H. E. Robertson, D. W. H. Rankin, and A. B. Altabef, *J. Raman Spectrosc.*, **41**, 1357–1368 (2010).
40. N. Subramania, N. Sundaraganesan, and J. Jayabharathi, *Spectrochim. Acta A*, **76**, 259–269 (2010).
41. P. Grunanger and P. V. Finzi, *The Chemistry of Heterocyclic Compounds, Isoxazoles*, John Wiley & Sons (1991).
42. S. Eryılmaz, M. Gül, E. İnkaya, and M. Taş, *J. Mol. Struct.,* **1108**, 209–222 (2016).
43. R. Y. Jin, X. H. Sun, Y. F. Liu, W. Long, B. Chen, S. Q. Shen, and H. X. Ma, *Spectrochim. Acta A*, **152**, 226–232 (2016).